Feasibility of nanoscale zero-valent iron loaded sediment-based biochar (nZVI-SBC) for simultaneous removal of nitrate and phosphate: high selectivity towards dinitrogen and synergistic mechanism

Xiaohui Liu
Beijing University of Technology
Jia Wei (1320926263@qq.com)
Beijing University of Technology
Liangang Hou
Beijing University of Technology
Yuhan Zhu
Beijing University of Technology
Yaodong Wu
Beijing University of Technology
Luyi Xing
Beijing University of Technology
Yifei Zhang
Beijing University of Technology
Jun Li
Beijing University of Technology

Research Article

Keywords: Sediment-based biochar, Nanoscale zero-valent iron, Nitrate, Phosphate, Simultaneous removal

Posted Date: February 12th, 2021

DOI: https://doi.org/10.21203/rs.3.rs-222879/v1

Version of Record: A version of this preprint was published at Environmental Science and Pollution Research on March 13th, 2021. See the published version at https://doi.org/10.1007/s11356-021-13322-w.

Feasibility of nanoscale zero-valent iron loaded sediment-based biochar (nZVI-SBC) for simultaneous removal of nitrate and phosphate: high selectivity towards dinitrogen and synergistic mechanism

Xiaohui Liu, Jia Wei*, Liangang Hou, Yuhan Zhu, Yaodong Wu, Luyi Xing, Yifei Zhang, Jun Li

College of Architecture Engineering, Beijing University of Technology, 100 Pingleyuan, Chaoyang district, Beijing 100124, China.

Corresponding author: weij@bjut.edu.cn (Jia Wei)

Declarations

Ethics approval and consent to participate: Not applicable.

Consent for publication: Not applicable.

Availability of data and materials: All data generated or analysed during this study are included in this published article and its supplementary information files.

Competing interests: The authors declare that they have no competing interests in this section.

Funding: All sources of funding for the research reported and The role of the funding body in the design of the study and collection, analysis, and interpretation of data and in writing the manuscript were declared in the manuscript.

Authors' contributions

X.H L. and J.W. designed the study, performed the research, analysed data, and wrote the paper. L.G. H., Y.H. Z., Y.D. W. and J. L. contributed significantly to analysis of the synergistic mechanism. L.Y. X. and Y.F. Z. helped perform the analysis with constructive discussions. All authors have read and approved the final manuscript.

Graphical abstract

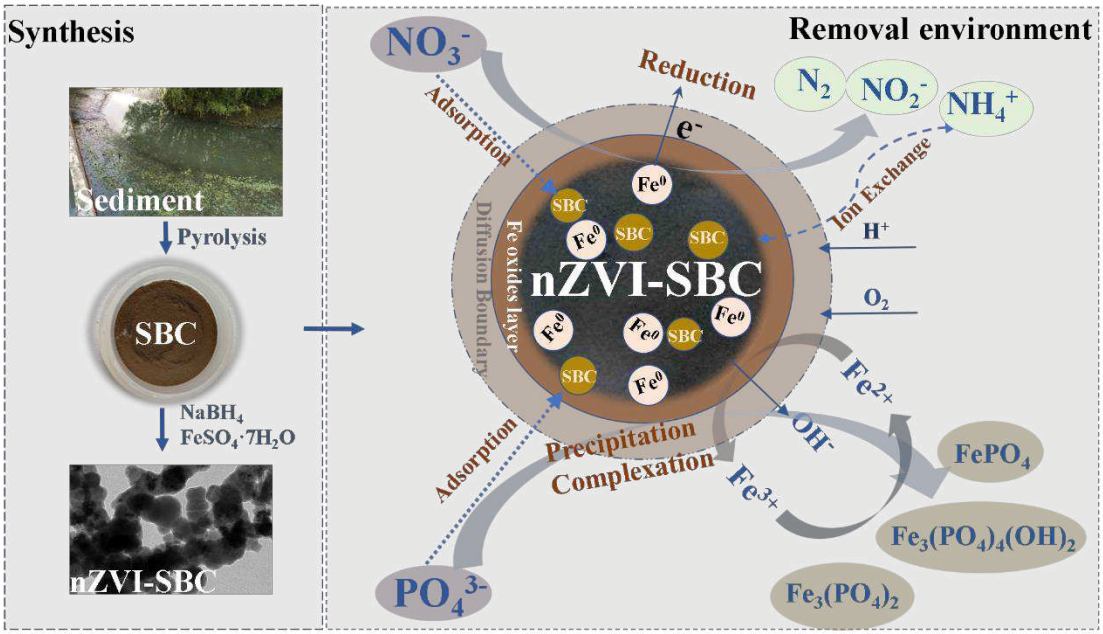

Abstract

In the process of water treatment, excessive nitrogen and phosphorus pollutants are of great concern. Therefore, we prepared nanoscale zero-valent iron loaded on sediment-based biochar (nZVI-SBC) to conduct nitrate and phosphate removal at the same time. The characterization demonstrated that nZVI-SBC was successfully synthesized, which had obvious advantages for larger specific surface area and better dispersion compared with pure nZVI. The batch experiments indicated that the best loading ratio of nZVI to SBC and optimum dosage for nitrate and phosphate were 1:1and 2 $g \cdot L^{-1}$, respectively. Their removal by nZVI-SBC was an acid-driven process. Anoxic environment was more conducive to the reduction of nitrate while the phosphate removal was fond of oxygen environment. 77.78% of nitrate and 99.21% of phosphate have been successfully removed, mainly depending on reduction and complexation mechanism, respectively. Moreover, nZVI-SBC had higher N_2 selectivity and produced less ammonium than nZVI. The interaction between nitrate and phosphate was studied to manifest that they had different degrees of inhibition during the removal of the other. Our research indicated that nZVI-SBC has great potential for remediation of nitrogen and phosphorus polluted water.

Keywords: Sediment-based biochar; Nanoscale zero-valent iron; Nitrate; Phosphate; Simultaneous removal

Introduction

Nitrogen (N) and phosphorus (P) are abundant in the water body because of human activities (Yin et al. 2018b). Eutrophication caused by nitrogen and phosphorus leads

to water hypoxia, resulting in the death of a large number of fish and plants, thus affecting the water environment. In order to reduce the negative impacts of ecosystem overburden, researchers have developed many techniques for the treatment of water with high concentrations of nitrate and phosphate (e.g., ion exchange, filtration / reverse osmosis, biological process, chemical removal) (Oh et al. 2016). Chemical removal would be more economically viable, and fit for in-situ remediation of nitrate and phosphate from wastewater better compared with other methods.

Nanoscale zero-valent iron (nZVI) exhibits large active surface, high diffusion activation energy and strong quantum effect (Wang et al. 2019). Up to now, various contaminants including antibiotics, chlorinated organics, heavy metals, and dyes have already been effectively removed in nZVI-based processes (Diao et al. 2019). Due to the strong reduction, precipitation and complexation ability of nZVI, it has been also attempted to remove nitrate and phosphate. 98.9% of phosphate was removed from aqueous solution with nZVI (Wen et al. 2014), which suggested notably higher and better uptake of phosphate via nZVI in adsorption and coprecipitation processes. NZVI was also used to remove 39% of nitrate (Wei et al. 2018), indicating reducibility and tendency of aggregation of nZVI. However, the application of nZVI faces the challenges of thermodynamic instability, easy oxidation, short reaction duration, poor air stability and rapid agglomeration (Yang et al. 2018).

It is an effective strategy to promote the performance of nZVI by assembling suitable porous supports. Montmorillonite (Zhao et al. 2018), rectorite (Luo et al. 2013), bentonite (Diao et al. 2016), kaolinite (Li et al. 2016) and zeolite (He et al. 2018) are

all reported as potential loaded materials. Biochar (BC) as a kind of powder material obtained by pyrolysis of biomass at high temperature in an oxygen-limited environment is paid close attention for high specific surface area, stable construction, and good electrical conductivity (Keiluweit et al. 2010). BC can adsorb pollutants and decrease their biological availability due to the interaction between functional groups (acidity/basicity) and electron transfer promoted by π-π bond. These properties enable nZVI to adjust and optimize nanoparticles in the corrosion rate, dispersion, particle size, and electron transfer capacities (Jiang et al. 2018). The utilization of BC to support nZVI as a porous carrier enhances the reactivity of nZVI (Oleszczuk &Koltowski 2017), prolongs its lifetime and improves the electron transfer efficiency (Cao et al. 2020). Furthermore, it is conducive to the resource recovery of biological waste and economically beneficial.

In the previous studies, many kinds of biomass materials such as corn stalks (Liu et al. 2018), cyanobacteria (Jiang et al. 2018), kenaf bark (Zhu et al. 2018), coconut shell and excess sludge (Wei et al. 2019) have been made into BC. However, BC made from river sediment is rarely studied. The sediments contain large number of biomass, which can be a novel choice to be used as raw materials for carbonization synthesis of BC (Yin et al. 2018a). Making biochar from sediment at high temperature not only avoids secondary pollution and land waste caused by sediment composting, ensuring the stability and harmlessness of sediment, but also benefits from lower cost and more reasonable economy compared with making sediment into filling materials, building materials and graded resource utilization. In addition, the composition of sediment is

different from that of other biomass, which leads to great changes in its properties. In particular, its interaction with nZVI may vary greatly. As far as we know, few studies were related to sediment-based biochar and simultaneous removal of nitrate along with phosphate by nZVI-BC. Therefore, it brings great challenges to this research.

In this study, we took use of prepared sediment-based biochar (SBC) supported nZVI (nZVI-SBC) to synchronous removal of nitrate and phosphate and investigate synergistic affect between them. The research objectives were (1) to discover the specific properties of newly synthesized nZVI-SBC by a series of characterization methods, (2) to figure out the effects on removal of nitrate and phosphate, (3) to explore the mechanism of interrelation between nitrate and phosphate under the simultaneously removal by nZVI-SBC. The results of this study not only provide a better understanding of interaction between nitrate and phosphate commendably for us to optimize nZVI-BC's application scenarios, but also show more possibilities for sediment resource utilization.

2. Materials and methods

2.1. Preparation and characterization of nZVI-SBC

The sediment was sampled from the esturary of the Tonghui River (39°54′20″N; 116°33′11″E), which is a polluted river connecting the Gaobeidian sewage treatment plant (Beijing, China). SBC was produced by 20 g of dry sediment under a 4-hour-pyrolyzation at 400 °C in a muffle furnace with the protection of nitrogen. NZVI-SBC was obtained in one step by liquid phase reduction by SBC, $FeSO_4 \cdot 7H_2O$, and $NaBH_4$ and further analyzed by of a series of characterization approaches including scanning

electron microscopy (SEM), transmission electron microscopy (TEM), Brunauer-Emmett-Teller (BET), X-ray diffraction (XRD), fourier transformation infrared spectroscopy (FTIR), X-ray photoelectron spectroscopy (XPS) and Zeta potentials. Supplementary material showed the details of materials and methods including preparation and characterization parameters of nZVI-SBC.

2.2. Batch experiments

The following nitrate and phosphate removal experiments were conducted in 50 mL sealed conical flask at 25 °C with 160 rpm shaking for 24 h to ensure equilibrium. After regular sampling and 0.22 μm membrane filtration, the nitrate, nitrite, ammonium and phosphate concentration was analyzed. The average of the three replicate samples represented the reported measurements below.

Effects of operational parameters: Nitrate and phosphate solution were prepared at the initial concentration range of 20-100 $mg \cdot L^{-1}$ and 5-50 $mg \cdot L^{-1}$. Impacts of nZVI-SBC ratios (1:4, 1:2, 1:1, 2:1, 4:1), dosage of nZVI-SBC (0.5-3.5 $g \cdot L^{-1}$), initial pH (pH_i) (3-11) and DO (0.3-9 $mg \cdot L^{-1}$) on the removal were examined in 25 mL solution (20 NO_3^--N $mg \cdot L^{-1}$ and 5 PO_4^3-P $mg \cdot L^{-1}$).

Interaction of nitrate and phosphate: In order to inquire the influence of nitrate on phosphate removal under the action of nZVI-SBC, the 10 $mg \cdot L^{-1}$ initial concentration of phosphate was controlled, and nitrate concentration was adjusted to 0, 10, 20, 50 and 100 $mg \cdot L^{-1}$, respectively. Then, fixed 20 $mg \cdot L^{-1}$ of nitrate was effected by phosphate concentration of 0, 5, 10, 20 and 50 $mg \cdot L^{-1}$.

Kinetic experiment: The kinetic study was proceeded in the 25 mL nitrate and

171 phosphate solution (20 NO_3^--N mg·L^{-1}, 5 PO_4^3-P mg·L^{-1}) and the samples were taken
172 out from conical flasks on the shaker one by one and filtered to be tested at the specified
173 time interval.

174 2.3. Analytical methods

175 During common nitrate reduction process, NO_2, N_2, NO_2^-, NH_4^+, NO and N_2O were
176 formed. As a matter of fact, the type of nitrate reduction products was strongly
177 dependent on the experimental conditions (Jung et al. 2014). The results showed that
178 NO and N_2O were generally formed under the condition of catalyst hydrogenation
179 (Liou et al. 2009). Hence, the production of NO_x and N_2O was assumed to be ignored.
180 We detected only NO_2^- and NH_4^+ in the solution and supposed that the rest products
181 were N_2 after considering all the possible products. The measurement and calculation
182 methods of nitrate, phosphate, ammonium and nitrite are shown in detail in the
183 supplementary material.

184 **3. Results and discussion**

185 3.1. Characterization

186 3.1.1. Morphological characteristics

187 As shown in Fig. 1, the surface of the original dry sediments was dense and flat,
188 with few pores and fractures. On the contrary, it was found that the porosity of the
189 product could be greatly improved by carbonizing sediment at high temperature. NZVI
190 as a whole presented distinct chain structure and individual particles of nZVI were
191 difficult to distinguish. The undoped nZVI particles tended to agglomerate due to their
192 magnetism and nano scale. The spherical black nanoparticles were dispersed on SBC's

surface, which confirmed that nZVI had good dispersion on SBC. It showed that SBC could inhibit nZVI from agglomeration and improve its dispersion and valid reactivity. As for nZVI-SBC, C, O, Si and Fe were widely distributed in the whole region.

3.1.2. XRD

From the XRD images (Fig. 2), we could find that the stronger peak at $2\theta = 30.99°$ was graphite crystal and the weaker diffraction peaks at $2\theta = 24.24°$, 25.66° and 59.08° were assigned to amorphous carbon structure as the typical characteristic for SBC and nZVI-SBC, indicating that the graphitization degree of SBC was relatively high. From the XRD analysis of nZVI-SBC, the higher peak at $2\theta = 52.14°$ represented more Fe^0 formed on the surface of SBC than pure nZVI. Peaks valued at 35.58° (Fe_2O_3), 35.46° (Fe_3O_4) and 44.84° ($Fe(OH)_3$) confirmed a smaller portion of iron oxides and hydroxides produced in Fe^0 oxidation during preparation or preservation. SBC played an important role in nZVI corrosion inhabitation.

3.1.3. FTIR

Fig. 3 showed the FTIR analysis of the functional groups of the synthesized materials from the wavelength range of 400 to 4000 cm^{-1}. The stretching and bending vibration peaks of O-H could be found at the characteristic peaks near 1625 and 3423 cm^{-1} (Kayan et al. 2017), and the peaks at 1415 and 1436 cm^{-1} were attributed to the skeleton vibration peak of aromatic ring or C=C vibration peak (Nguyen et al. 2015). The bands at 1030 and 1103 cm^{-1} were corresponding to C-O stretching vibration. The bands at 462, 467, 778 and 792 cm^{-1} went to the Si-O stretching vibration peak. The functional group types of SBC remained unchanged after loading nZVI. In the infrared

215 spectra of nZVI and nZVI-SBC, the Fe-O stretching vibration peaks of Fe_2O_3 and Fe_3O_4
216 corresponded to the bands around 617 and 620 cm^{-1}, indicating that nZVI was slightly
217 oxidized (Li et al. 2017).
218 3.1.4. XPS
219 After XPS characterization, it can be seen that the functional organic group C-C,
220 C=C, C-O and C=O contained on the surface of SBC still existed after loading (Fig. 4a,
221 4b). The differences between iron species of nZVI (Fig. 4c) and nZVI-SBC (Fig. 4d)
222 surface were compared by XPS peak analysis. The results showed that the Fe^0 area of
223 nZVI and nZVI-SBC samples accounted for 6.20% and 9.70% respectively. There can
224 be also observed less iron oxides assigned to Fe_2O_3 and Fe_3O_4 on the surface of nZVI-
225 SBC than pure nZVI, which indicated that SBC could improve the stability of nano
226 particles and inhibit the oxidation trend.
227 3.1.5. Zeta potential
228 The significance of Zeta potential is that the value is highly related to the material
229 dispersion stability. Zeta potentials of nZVI and nZVI-SBC were shown in Fig. 5. At
230 the same pH value, the isoelectric point of nZVI was higher at 7.42, and that of nZVI-
231 SBC moved to 6.73, indicating that electrostatic repulsion in nZVI-SBC particles was
232 greater and the system was more stable (Sheng et al. 2015). Therefore, nZVI could be
233 dispersed uniformly on SBC, and the aggregation tendency was weak.
234 3.2. Effects of operating conditions on the removal
235 3.2.1. Effect of synthesis ratio of nZVI-SBC
236 As BET analysis showed, SBC has a large surface area. However, the adsorption

on biochar surface is mainly due to electrostatic interaction. Only 1.16% of nitrate was removed as the negative charged SBC rarely adsorbed nitrate anion as shown in Fig.6a. NZVI had more advantages in nitrate removal (33.30%) than SBC due to its reducibility and adsorption capacity. Furthermore, compared with pure SBC and nZVI, the removal of nitrate by nZVI-SBC was significantly more improved, which effect was far better than that of SBC and nZVI alone. NZVI-SBC (1:1) had the highest removal efficiency of 77.78% among all nZVI-SBCs. Its superiority removal effect was mainly due to the more uniform distribution of iron particles and more active sites. The removal of phosphate was more easily. In addition to SBC's only 15.70% phosphate removal, the removal efficiency of other samples could reach more than 90%.

3.2.2. Effect of dosage of nZVI-SBC

As Fig. 5b depicted, with the increase of the dosage from 0.5 $g \cdot L^{-1}$ to 3.5 $g \cdot L^{-1}$, it had a positive correlation with nitrate and phosphate removal efficiency. Actually, as the dosage increased, more Fe^0 active sites and adsorption space were provided, promoting nitrate reduction and adsorption. Especially, for phosphate, only 0.5 $g \cdot L^{-1}$ dosage could get 97.14% removal effect. However, the trend of removal rate and removal capacity varied with the change of dosage. For nitrate, the removal capacity reached the maximum of 7.778 $mg \cdot g^{-1}$ when the dosage was 2 $g \cdot L^{-1}$ and then began to decline (Fig. S1). Therefore, the optimal dosage for this study was 2 $g \cdot L^{-1}$.

3.2.3. Effect of initial pH in solution

Effect of initial solution pH (pH_i) on simultaneous removal by nZVI-SBC were explored from 3.0 to 11.0 in Fig.6c. Nitrate removal was highest under the most acidic

conditions at pH_i 3 (86.86%). There was a slight decrease to 77.78% in a neutral environment at pH_i 7 and a more severe drop of 34.70% at pH_i 11. The removal efficiency was affected by the isoelectric point (about 6.73) to a great extent. The surface of nZVI-SBC was positively charged when the solution pH was lower than 6.73, and then negatively charged nitrate was easily adsorbed. Moreover, lower pH of solution would prevent the coating of ferrous hydroxide on the nZVI-SBC surface, yielding more nitrate reduction reaction sites. When the pH value of the solution was above the isoelectric point, the nitrate removal rate decreased due to the negative charge and electrostatic repulsion of nZVI-SBC. Then iron hydroxide precipitated in alkaline environment, leading to formation of a $Fe(OH)_2$ and $Fe(OH)_3$ layer deactivated the nZVI-SBC. It is worth noting that the pH of the solution increased to more than 8.0, and the final equilibrium pH was between 8.01 and 9.33. The nitrate reduction process was H^+ consumption and OH^- accumulation reaction. In addition, with the increase of pH_i, the amount of ammonium reduced and nitrite accumulated slightly (Fig.S2).

The decrease of phosphate removal rate with increased pH_i was related to electrostatic repulsion as well. In addition, the surface protonation of nZVI-SBC was conducive to the complexation and coprecipitation reaction with phosphate under acidic conditions. During the reaction process, Fe^{3+} and Fe^{2+} on the surface of nZVI-SBC could form ferric hydroxide, then further co-precipitated with phosphate. To summarize, nitrate and phosphate removal by nZVI-SBC is an acid-driven process. However, both of them can achieve high removal rate and the conditions are more practical at pH_i 7. Therefore, the following reactions are carried out at pH_i 7.

281 3.2.4. Effect of dissolved oxygen concentrations

282 The simulation of anaerobic to aerobic environment was carried out with different
283 concentrations of DO from 0.3 to 9 $mg \cdot L^{-1}$ in Fig. 6d. Anaerobic conditions are more
284 beneficial to nitrate removal. Both O_2 and nitrate could accept electron, but nZVI-SBC
285 preferred O_2 as an electron acceptor instead of nitrate. This yielded iron oxides forms,
286 such as Fe_3O_4, FeOOH and Fe_2O_3 on the nZVI-SBC surface, which might drop the
287 reactivity of nZVI and hinder further removal of nitrate over time. Additionally, Fig. S3
288 showed nitrite production after reaction equilibrium was very scarce under whether
289 anaerobic or aerobic conditions. Nitrate was mainly converted into N_2 and ammonium.
290 However, there was a slight increase in phosphate removal with DO raised. As a result
291 of low crystallinity and crystal defects of Fe, the increase of oxygen concentration
292 accelerated the corrosion of nZVI and enhanced the complexation and coprecipitation
293 of phosphate with iron.

294 3.3. The interaction between nitrate and phosphate

295 The increase of phosphate content was obviously disadvantageous to nitrate
296 reduction (Fig.7a). This could be because the increased phosphate reacts with iron
297 rapidly, forming an inner sphere complex on the surface of nZVI-SBC, resulting in the
298 decrease of active sites and the hindrance of the contact of nZVI-SBC with nitrate.
299 Nevertheless, the increase of phosphate concentration had little inhibition on the
300 removal of phosphate (Fig.7b), and phosphate was able to achieve a good removal
301 effect, which showed that phosphate and nZVI-SBC had a very strong ability of
302 complex adsorption and coprecipitation.

However, with the increase of initial nitrate concentration, the removal of nitrate and phosphate was inhibited to different extent. As the number of active sites and adsorption centers of nZVI-SBC was limited, nitrate removal efficiency decreased (Fig.7c). As for phosphate, the increase of nitrate promoted the consumption of nZVI and H^+, and the negative charge accumulated in the solution. Due to the electrostatic repulsion, it was not conducive to the adsorption of phosphate on the surface of the material. However, increased nitrate also made more nZVI form iron oxide and iron hydroxide. Phosphate could coprecipitate with more products, enhancing its removal. Obviously, the inhibition was stronger than promotion, so nitrate could inhibit the removal of phosphate in the reaction system(Fig.7d).

3.4. Kinetics

The experimental data of nitrate and phosphate removal were further revealed by the first-order and the second-order equations (Fig. 9a, 9b) (Wei et al. 2018). . The reaction equation was expressed in Eq. (1-2):

$$-\frac{\mathrm{d}C_\mathrm{t}}{dt} = kC_\mathrm{t}^\mathrm{n} \quad (1)$$

$$\frac{1}{C_\mathrm{t}^{\mathrm{n}-1}} - \frac{1}{C_0^{\mathrm{n}-1}} = (n-1)kt \quad (2)$$

where C_t represents the residual concentration, K was the rate constant, n went to the reaction series, and C_0 was initial concentration. The first-order and second-order reaction models were fitted to the kinetic data. Table 1. displayed the fitted parameters.

The good fit of data for nitrate removal to the linear model provided a strong evidence that the reaction was a first-order model reaction. The process required equilibrium time of 12 h. Such lumped parameters embedded many physical processes

in the nitrate adsorption. The chemical reaction of nZVI-SBC to phosphate was more suitable for the second-order kinetic model due to its relatively higher R^2 than the first-order kinetic model (0.997 versus 0.978). The results indicated that the chemisorption was the dominant factor in the adsorption of phosphate by the nZVI-SBC. The reaction needed a shorter equilibrium time of 6 h, and the constant was 0.047 [$(mg \cdot L)^{1-n} \cdot min^{-1}$].

3.5. N_2 selectivity

Performance of nZVI and nZVI-SBC on N_2 selectivity was studied. The N_2 selectivity at equilibrium may be the result of competition between NH_4^+ selectivity rate and N_2 selectivity rate. The sum of generated N_2 and adsorbed NH_4^+ were recognized as an equivalent N_2 selectivity. In the nZVI removal system, 94.31% of the reduced nitrate converted into ammonium, while only 4.32% accounted for N_2. For nZVI-SBC, 41.77% and 57.14% of nitrate corresponded to ammonium and N_2 respectively. Obviously, the nZVI-SBC exhibited higher N_2 selectivity. The reduction of nitrate was a gradual process: firstly, nitrate was reduced to nitrite with Fe^0, Fe^{2+} and other reducing agents, and then converted into NH_4^+ or N_2. Meanwhile, a micro battery with nZVI as anode and SBC as cathode could be formed spontaneously on nZVI-SBC materials, promoting the transfer of electrons to NO_3^- and accelerated the reduction. The relative potential difference could shorten intragranular diffusion resistance and drive the reduction of nitrite to N_2. In addition, SBC could also be used as a good adsorbent for NH_4^+ to improve N_2 selectivity. NZVI-SBC could have a close N_2 selectivity compared with metal-mixed nZVIs (Krasae &Wantala 2016). However, supporting SBC was much cheaper and more realistic than those doped metals. Hence,

the higher N_2 selectivity by nZVI-SBC not only has important theoretical significance, but also huge potential economic benefit.

3.6. Nitrate and phosphate simultaneous removal mechanism

When nZVI particles were supported on SBC, they exhibited good dispersion, small particle size and high reaction activity. In addition, some Fe^0 particles restricted or bound in the inner pore still remained active due to the microporous characteristics of SBC, despite the formation of iron oxide layer on nZVI-SBC. Moreover, SBC conducted electricity in oxidation and reduction reactions and provided conditions for diffusion and migration of molecules to iron active sites by promoting long-range electron transport.

The process of nitrate removal by nZVI involves the transfer of electrons between nZVI and the oxidizing species (O_2, H^+, and nitrate) (Guan et al. 2015). The whole process of electron transfer usually involved a series of steps, including the migration of O_2, H^+, and nitrate from solution to nZVI-SBC surface, the reaction among them, and the diffusion of products (Fe^{3+}, Fe^{2+} and OH^-) into the solution. The removal process could be described via Eqs. (3)-(9). Furthermore, the micro battery formed spontaneously by SBC and nZVI accelerated the electron transfer and promoted the effective removal of nitrate. Ion exchange reaction could make NH_4^+ or nitrite products adsorbed by SBC, reducing nitrate to a greater extent and improving the selectivity of N_2.

$$Fe^0 + NO_3^- + 2H^+ \rightarrow Fe^{2+} + NO_2^- + H_2O \quad (3)$$

$$3Fe^0 + NO_2^- + 8H^+ \rightarrow 3Fe^{2+} + NH_4^+ + 2H_2O \quad (4)$$

369 $3Fe^0 + 2NO_2^- + 8H^+ \rightarrow 3Fe^{2+} + N_2 + 4H_2O$ (5)

370 $5Fe^0 + 2NO_3^- + 6H_2O \rightarrow 5Fe^{2+} + N_2 + 12OH^-$ (6)

371 $Fe^0 + 2H_2O \rightarrow Fe^{2+} + H_2 + 2OH^-$ (7)

372 $NO_3^- + 2H^+ + 4H_2 \rightarrow NH_4^+ + 3H_2O$ (8)

373 $4Fe^0 + NO_3^- + 10H^+ \rightarrow 4Fe^{2+} + NH_4^+ + 3H_2O$ (9)

374 Phosphate could be significantly removed by nZVI-SBC. The mechanism of
375 phosphate removal contained adsorption, complexation and coprecipitation. As
376 mentioned in 3.2.3, the process of complexation and precipitation might play a major
377 role, while the electrostatic attraction mechanism was not dominant in alkaline
378 environment. As a result of the reaction between iron and water, a layer of hydroxide
379 including $Fe(OH)_2$, $Fe(OH)_3$, $FePO_4$, $Fe_3(PO_4)_2$ and $Fe_3(PO_4)_4(OH)_2$ (Fig. S4.) was
380 formed at the same time.

381 The adsorption, reduction, coprecipitation and complexation coexisted in the
382 removal process, but the four kinds of functions also affected each other in various ways.
383 Due to the limited attachment site and activity of nanomaterials, nitrate and phosphate
384 had different inhibition on each other's removal. However, nZVI-SBC could have ideal
385 removal effects for both.

386 **4. Conclusions**

387 In this study, we have successfully synthesized and used SBC as the carrier of nZVI
388 for simultaneous removal of nitrate and phosphate. SBC could significantly inhibit the
389 aggregation tendency of particles and prevent them from passivation. Nitrate and
390 phosphate removal were both favorable in acidic environment. Nitrate removal was

more efficient under anaerobic conditions, but phosphate preferred oxygen. NZVI-SBC mainly took advantage of its strong reducibility to fully remove nitrate, while the removal of phosphate depended on its complexation and co-precipitation with iron oxide and hydroxide. Nitrate and phosphate coexisted and antagonized each other, and finally reached a state of dynamic equilibrium. The micro battery formed by nZVI/SBC had the functions of redox, precipitation, adsorption and electrochemical capture. They all played an important role in the removal of target pollutants. Moreover, nZVI-SBC showed higher N_2 selectivity and less ammonium production than nZVI. The proposed synchronous removal process showed significant application potential for sediment-based biochar, which broadened the perspective for us to select adsorption materials, and successfully achieved the resource utilization of biomass waste. Furthermore, the successful combination of SBC and nZVI also had certain reference significance for water treatment.

Acknowledgements

Authors would like to acknowledge the financial support by the National Natural Science Foundation of China (51778015), Beijing Municipal Natural Science Foundation (8202007) and Major Science and Technology Program for Water Pollution Control and Treatment (2017ZX07103-001).

References

Cao Z, Li H, Xu XH, Xu J (2020): Correlating surface chemistry and hydrophobicity of sulfidized nanoscale zerovalent iron with its reactivity and selectivity for

414 denitration and dechlorination. Chem. Eng. J. 394, 124876.
415 https://doi.org/10.1016/j.cej.2020.124876
416 Diao ZH, Xu XR, Jiang D, Kong LJ, Sun YX, Hu YX, Hao QW, Chen H (2016):
417 Bentonite-supported nanoscale zero-valent iron/persulfate system for the
418 simultaneous removal of Cr(VI) and phenol from aqueous solutions. Chem. Eng.
419 J. 302, 213-222. https://doi.org/10.1016/j.scitotenv.2019.01.037
420 Diao ZH, Qian W, Lei ZX, Kong LJ, Du JJ, Liu H, Yang JW, Pu SY (2019): Insights on
421 the nitrate reduction and norfloxacin oxidation over a novel nanoscale zero
422 valent iron particle: Reactivity, products, and mechanism. Sci. Total Environ.
423 660, 541-549. https://doi.org/10.1016/j.cej.2016.05.062
424 Guan XH, Sun YK, Qin HJ, Li JX, Lo IMC, He D, Dong HR (2015): The limitations
425 of applying zero-valent iron technology in contaminants sequestration and the
426 corresponding countermeasures: the development in zero-valent iron
427 technology in the last two decades (1994-2014). Water Res. 75, 224-248.
428 https://doi.org/10.1016/j.watres.2015.02.034
429 He YH, Lin H, Dong YB, Li B, Wang L, Chu SY, Luo MK, Liu JF (2018): Zeolite
430 supported Fe/Ni bimetallic nanoparticles for simultaneous removal of nitrate
431 and phosphate: Synergistic effect and mechanism. Chem. Eng. J. 347, 669-681.
432 https://doi.org/10.1016/j.cej.2018.04.088
433 Jiang XY, Ouyang ZZ, Zhang ZF, Yang C, Li XQ, Dang Z, Wu PX (2018): Mechanism
434 of glyphosate removal by biochar supported nano-zero-valent iron in aqueous
435 solutions. Colloids Surf., A 547, 64-72.
436 https://doi.org/10.1016/j.colsurfa.2018.03.041
437 Jung SY, Bae SJ, Lee WJ (2014): Development of Pd–Cu/Hematite Catalyst for
438 Selective Nitrate Reduction. Environ. Sci. Technol. 48, 9651-9658.
439 https://doi.org/10.1021/es502263p
440 Kayan B, Khataee A, Kalderis D, Akay S, Konsolakis M (2017): Ultrasound-assisted
441 removal of Acid Red 17 using nanosized Fe3O4-loaded coffee waste
442 hydrochar. Ultrason. Sonochem. 35, 72-80.
443 https://doi.org/10.1016/j.ultsonch.2016.09.004

444 Keiluweit M, Nico PS, Johnson MG, Kleber M (2010): Dynamic Molecular Structure
445 of Plant Biomass-Derived Black Carbon (Biochar). Environ. Sci. Technol. 44,
446 1247-1253. https://doi.org/10.1021/es9031419
447 Krasae N, Wantala K (2016): Enhanced nitrogen selectivity for nitrate reduction on Cu-
448 nZVI by TiO2 photocatalysts under UV irradiation. Appl. Surf. Sci. 380, 309-
449 317. https://doi.org/10.1016/j.apsusc.2015.12.023
450 Li PJ, Lin KR, Fang ZQ, Wang KM (2017): Enhanced nitrate removal by novel
451 bimetallic Fe/Ni nanoparticles supported on biochar. J. Cleaner Prod. 151, 21-
452 33. https://doi.org/10.1016/j.jclepro.2017.03.042
453 Li XG, Zhao Y, Xi BD, Mao XH, Gong B, Li R, Peng X, Liu HL (2016): Removal of
454 Nitrobenzene by Immobilized Nanoscale Zero-valent Iron: Effect of Clay
455 Support and Efficiency Optimization. Appl. Surf. Sci. 370, 260-269
456 https://doi.org/10.1016/j.apsusc.2016.01.141
457 Liou YH, Lin CJ, Weng SC, Ou HH, Lo SL (2009): Selective Decomposition of
458 Aqueous Nitrate into Nitrogen Using Iron Deposited Bimetals. Environ. Sci.
459 Technol. 43, 2482-2488. https://doi.org/10.1021/es802498k
460 Liu CM, Diao ZH, Huo WY, Kong LJ, Du JJ (2018): Simultaneous removal of Cu~(2+)
461 and bisphenol A by a novel biochar- supported zero valent iron from aqueous
462 solution: Synthesis, reactivity and mechanism. Environ. Pollut. 239, 698-705.
463 https://doi.org/10.1016/j.envpol.2018.04.084
464 Luo S, Qin PF, Shao JH, Peng L, Gu JD (2013): Synthesis of reactive nanoscale zero
465 valent iron using rectorite supports and its application for Orange II removal.
466 Chem. Eng. J. 223, 1–7. https://doi.org/10.1016/j.cej.2012.10.088
467 Nguyen TC, Loganathan P, Nguyen TV, Vigneswaran S, Kandasamy J, Naidu R (2015):
468 Simultaneous adsorption of Cd, Cr, Cu, Pb, and Zn by an iron-coated Australian
469 zeolite in batch and fixed-bed column studies. Chem. Eng. J. 270, 393-404.
470 https://doi.org/10.1016/j.cej.2015.02.047
471 Oh SY, Seo YD, Kim B, Kim IY, Cha DK (2016): Microbial reduction of nitrate in the
472 presence of zero-valent iron and biochar. Bioresour. Technol. 200, 891-896.
473 http://dx.doi.org/10.1016/j.biortech.2015.11.021

Oleszczuk P, Koltowski M (2017): Effect of co-application of nano-zero valent iron and biochar on the total and freely dissolved polycyclic aromatic hydrocarbons removal and toxicity of contaminated soils. Chemosphere 168, 1467-1476. https://doi.org/10.1016/j.chemosphere.2016.11.100

Sheng G, Alsaedi A, Shammakh W, Monaquel S, Huang Y (2015): Enhanced sequestration of selenite in water by nanoscale zero valent iron immobilization on carbon nanotubes by a combined batch, XPS and XAFS investigation. Carbon 99, 123-130. https://doi.org/10.1016/j.carbon.2015.12.013

Wang S, Zhao M, Zhou M, Li YC, Wang J, Gao B, Sato S, Feng K, Yin W, Igalavithana AD, Oleszczuk P, Wang X, Ok YS (2019): Biochar-supported nZVI (nZVI/BC) for contaminant removal from soil and water: A critical review. J. Hazard. Mater 373, 820-834. https://doi.org/10.1016/j.jhazmat.2019.03.080

Wei Al, Ma J, Chen Jj, Zhang Y, Song JX, Yu XY (2018): Enhanced nitrate removal and high selectivity towards dinitrogen for groundwater remediation using biochar-supported nano zero-valent iron. Chem. Eng. J. 353, 595-605. https://doi.org/10.1016/j.cej.2018.07.127

Wei J, Liu YT, Li J, Zhu YH, Yu H, Peng YZ (2019): Adsorption and co-adsorption of tetracycline and doxycycline by one-step synthesized iron loaded sludge biochar. Chemosphere 236, 124254. https://doi.org/10.1016/j.chemosphere.2019.06.224

Wen Z, Zhang Y, Dai C (2014): Removal of phosphate from aqueous solution using nanoscale zerovalent iron (nZVI). Colloids Surf., A 457, 433-440. https://doi.org/10.1016/j.colsurfa.2014.06.017

Yang F, Zhang S, Sun Y, Cheng K, Li J, Tsang DCW (2018): Fabrication and characterization of hydrophilic corn stalk biochar-supported nanoscale zero-valent iron composites for efficient metal removal. Bioresour. Technol. 265, 490-497. https://doi.org/10.1016/j.biortech.2018.06.029

Yin HB, Zhu JC, Tang WY (2018a): Management of nitrogen and phosphorus internal loading from polluted river sediment using Phoslock® and modified zeolite with intensive tubificid oligochaetes bioturbation. Chem. Eng. J. 353, 46-55. https://doi.org/10.1016/j.cej.2018.07.112

504 Yin Q, Ren H, Wang R, Zhao Z (2018b): Evaluation of nitrate and phosphate adsorption
505 on Al-modified biochar: Influence of Al content. Sci. Total Environ. 631-632,
506 895-903. https://doi.org/10.1016/j.scitotenv.2018.03.091
507 Zhao YF, Cao X, Song XS, Zhao ZM, Wang YH, Si ZH, Lin FD, Chen Y, Zhang YJ
508 (2018): Montmorillonite supported nanoscale zero-valent iron immobilized in
509 sodium alginate (SA/Mt-NZVI) enhanced the nitrogen removal in vertical flow
510 constructed wetlands (VFCWs). Bioresour. Technol. 267, 608-617.
511 https://doi.org/10.1016/j.biortech.2018.07.072
512 Zhu YE, Hua L, Zhang GX, Meng FJ, Li LF, Wu S (2018): Removal of hexavalent
513 chromium from aqueous solution by different surface-modified biochars: Acid
514 washing, nanoscale zero-valent iron and ferric iron loading. Bioresour. Technol.
515 261, 142-150. https://doi.org/10.1016/j.biortech.2018.04.004
516

Figures

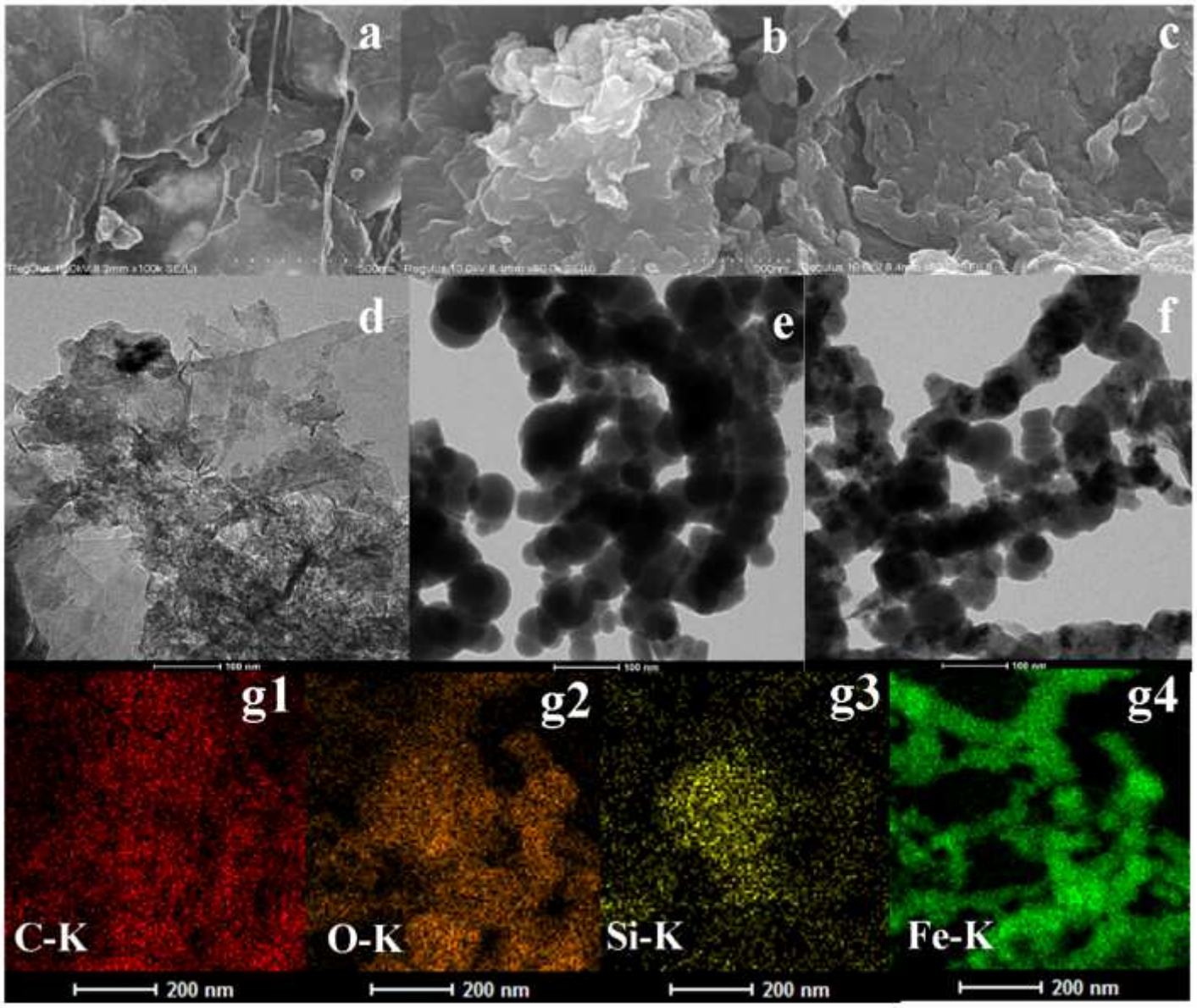

Figure 1

Electron microscope images and elemental mapping (a. SEM of pristine sediment; b. SEM of SBC; c. SEM of nZVI-SBC; d. TEM of SBC; e. TEM of nZVI; f. TEM of nZVI-SBC; g. elemental mapping of nZVI-SBC).

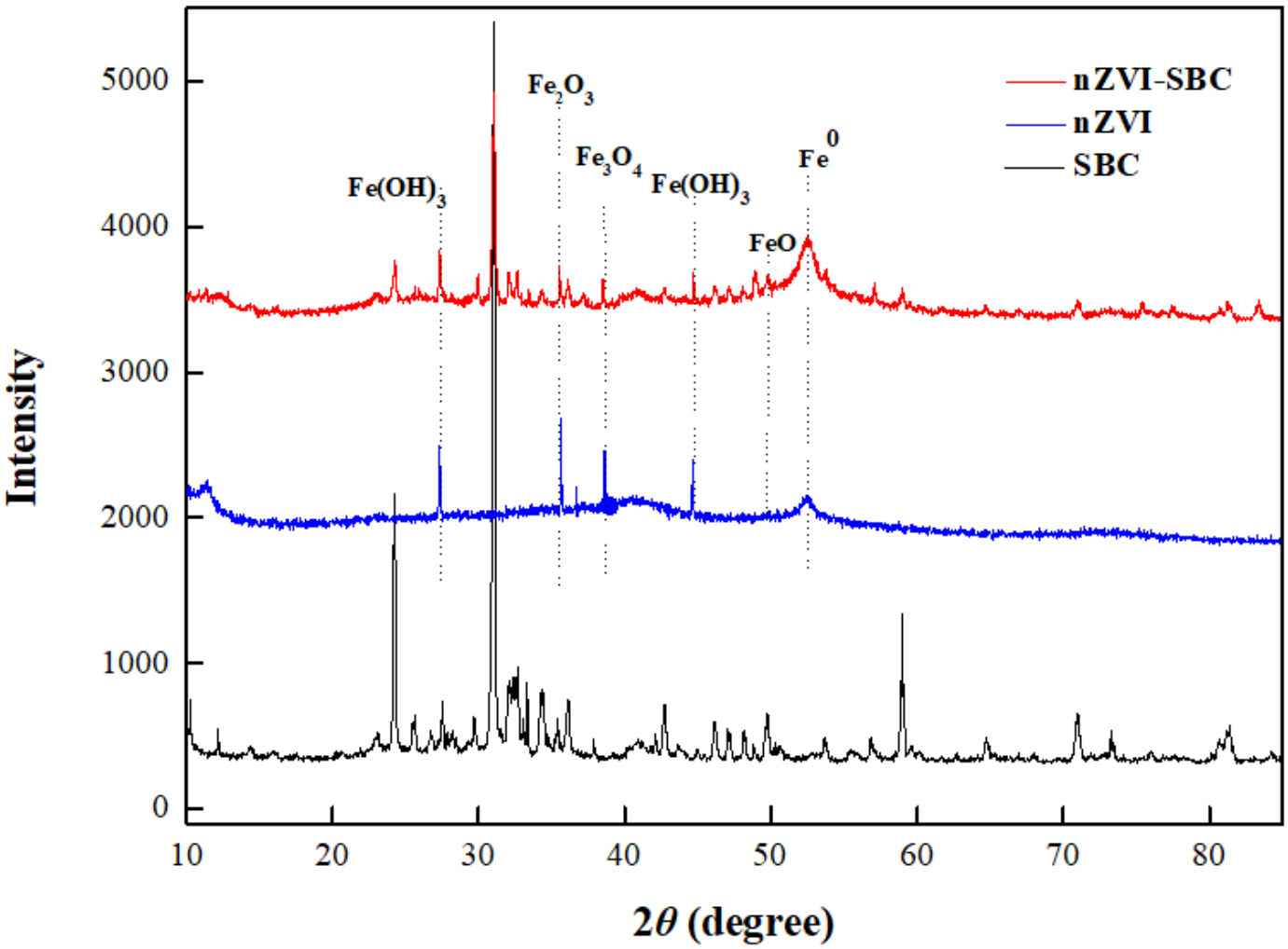

Figure 2

X-ray diffraction patterns of SBC, nVZI-SBC and nZVI.

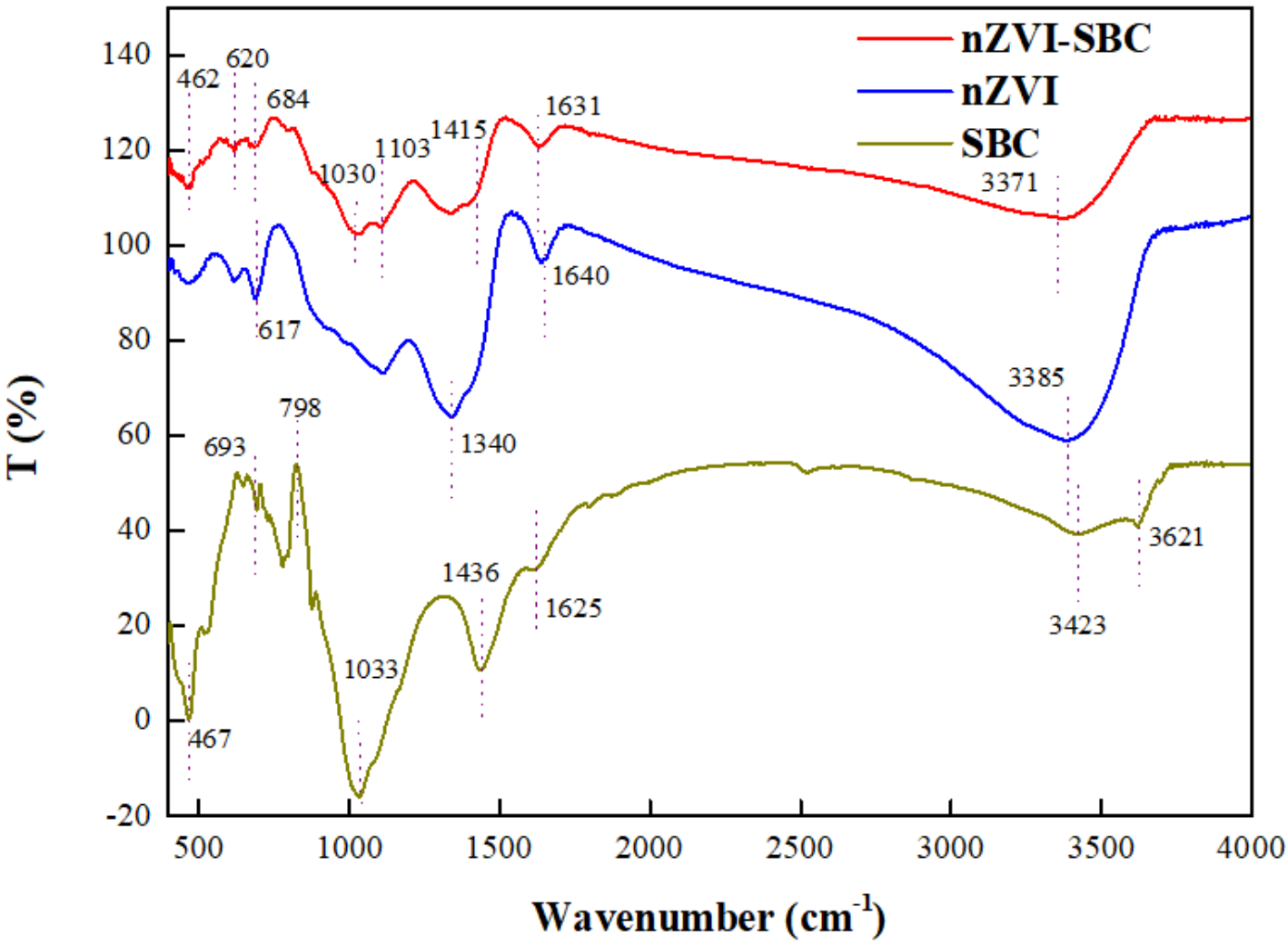

Figure 3

Fourier transform infrared spectra (a. SBC; b. nZVI-SBC; c. nZVI).

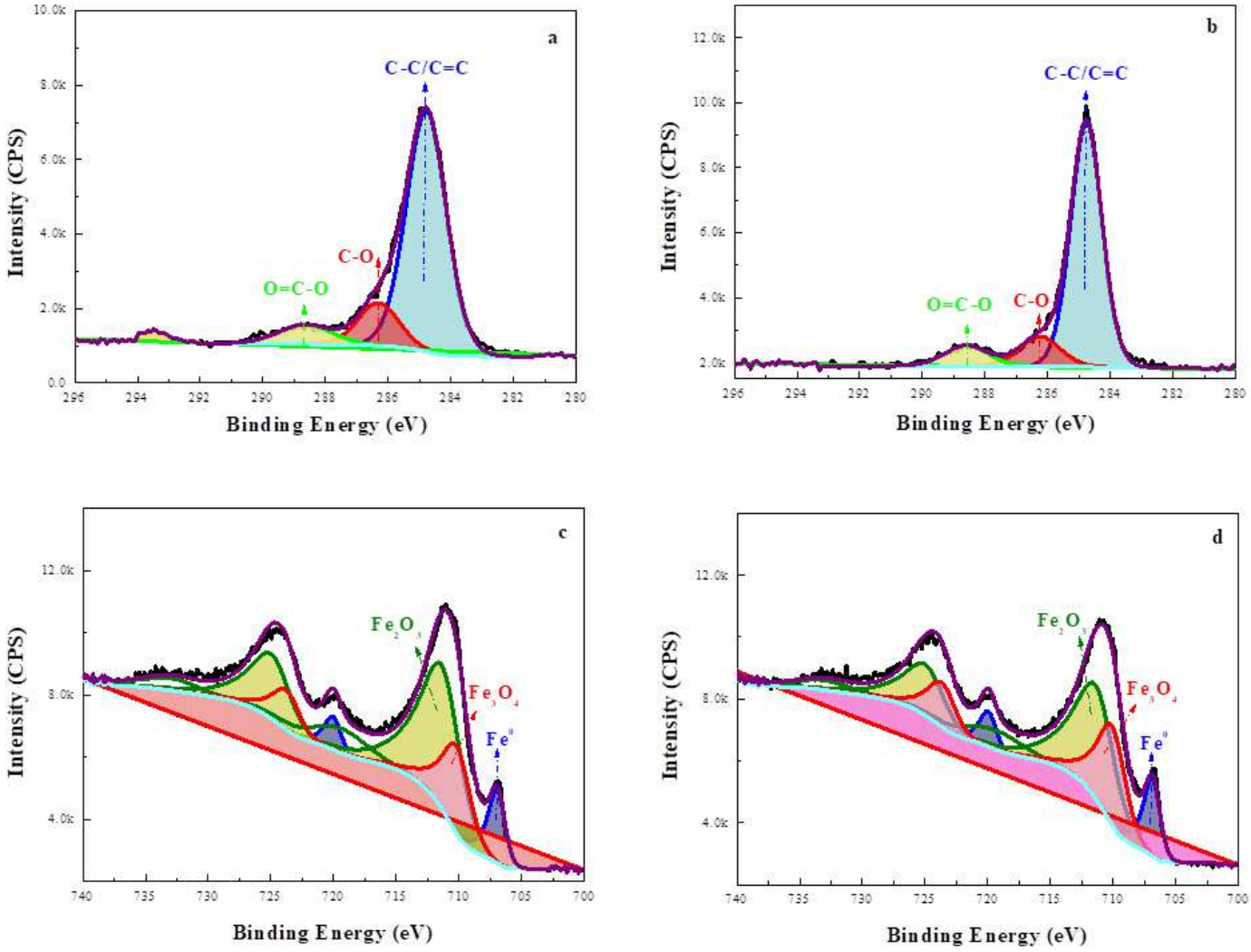

Figure 4

XPS images of C, O analysis (a. SBC; b. nZVI-SBC) and Fe analysis (c. nZVI; d. nZVI-SBC.

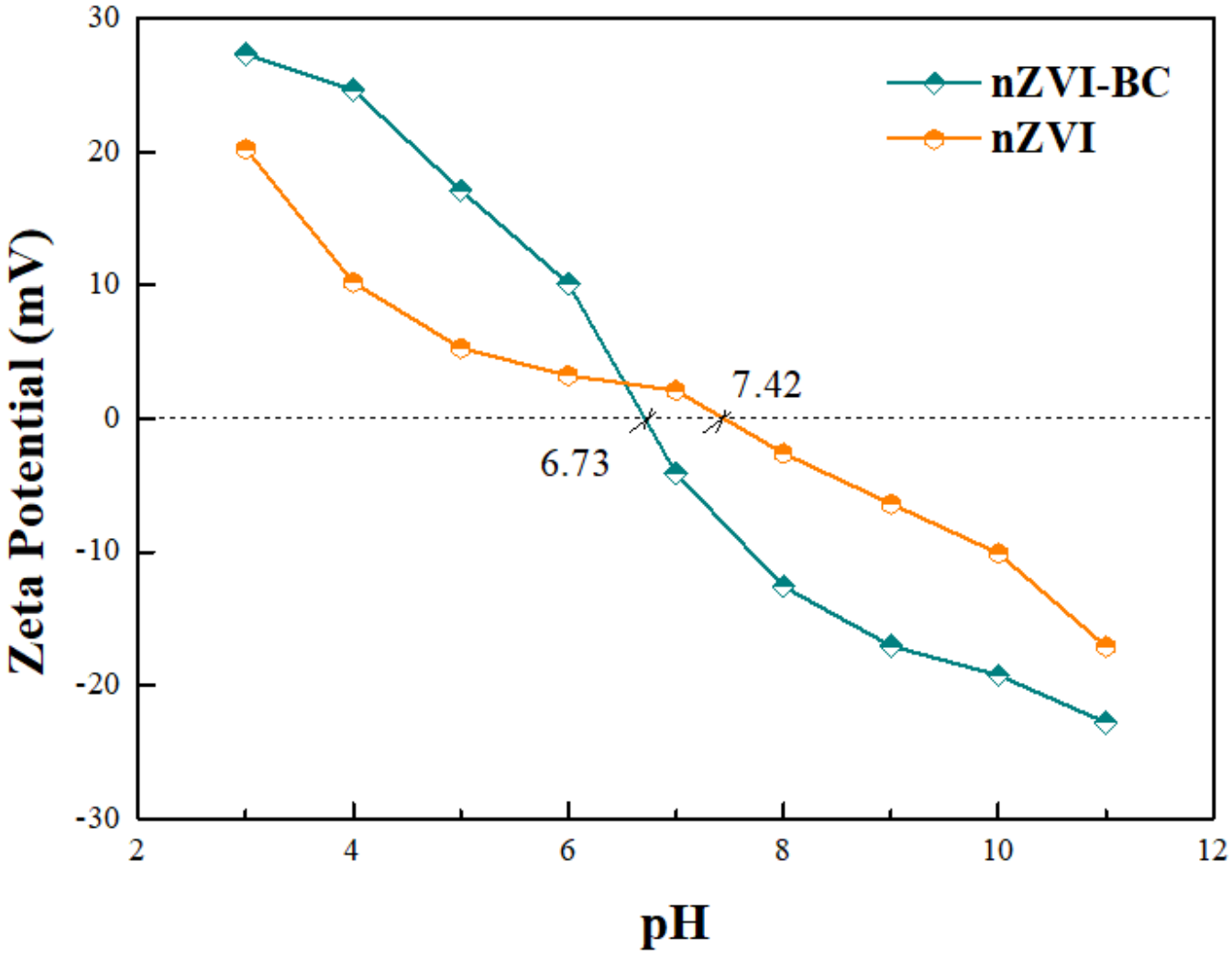

Figure 5

Zeta potential of nZVI-SBC and nZVI.

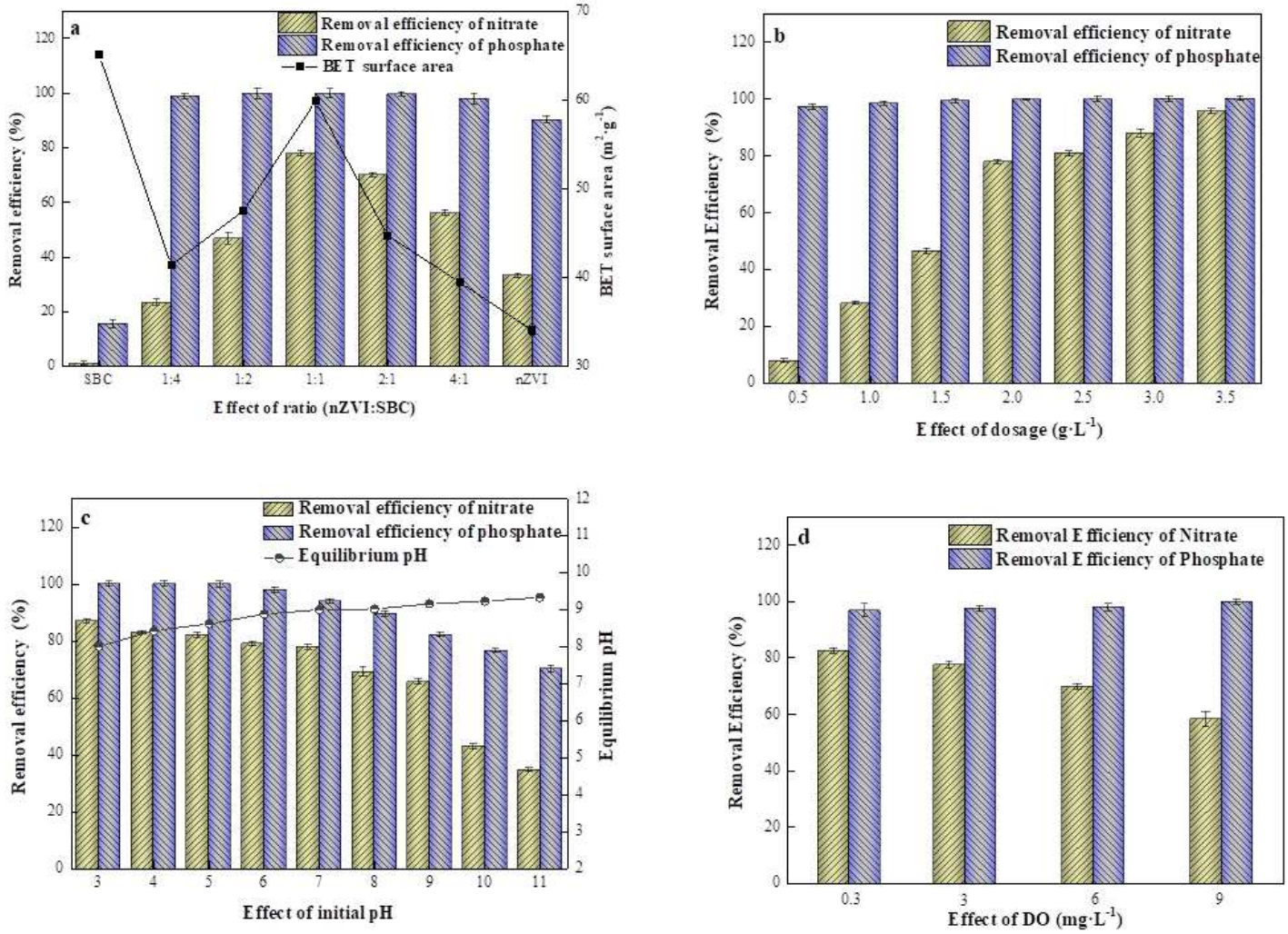

Figure 6

Effects on the removal of nitrate and phosphate (20 NO3−-N mg·L-1, 5 PO43-P mg·L-1): a. mass ratio of Fe0 (pH = 7, DO = 3 mg·L-1, dosage = 2g·L-1); b. dosage (pH = 7, DO = 3 mg·L-1); c. initial solution pH (dosage = 2g·L-1, DO = 3 mg·L-1); d. DO (dosage = 2 g·L-1, pH = 7).

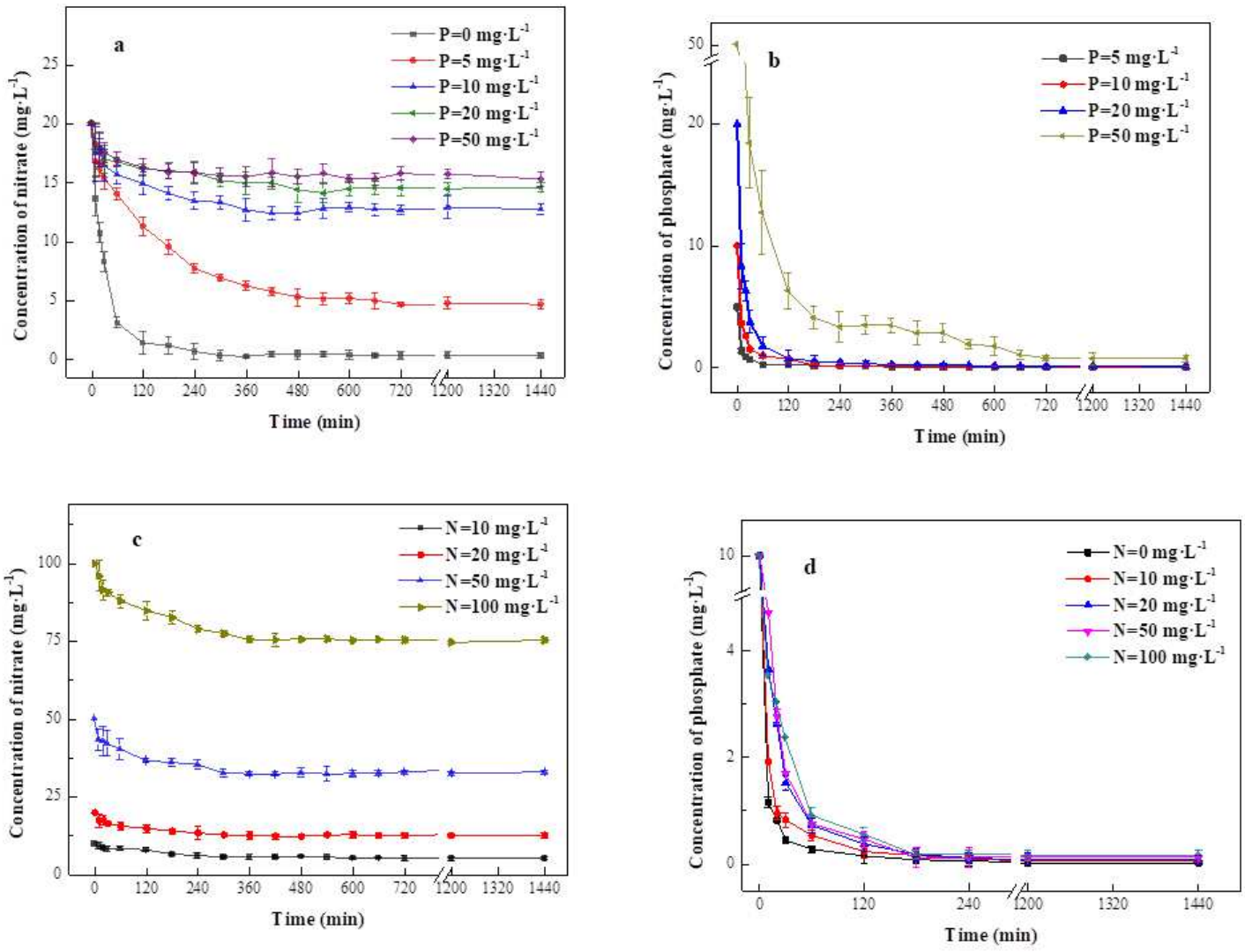

Figure 7

The influence of phosphate concentration (dosage = 2 g·L-1, pH = 7, DO = 3 mg·L-1): a. nitrate removal, b. phosphate removal; the influence of nitrate concentration (dosage = 2 g·L-1, pH = 7, DO = 3 mg·L-1): c. nitrate removal, d. phosphate removal.

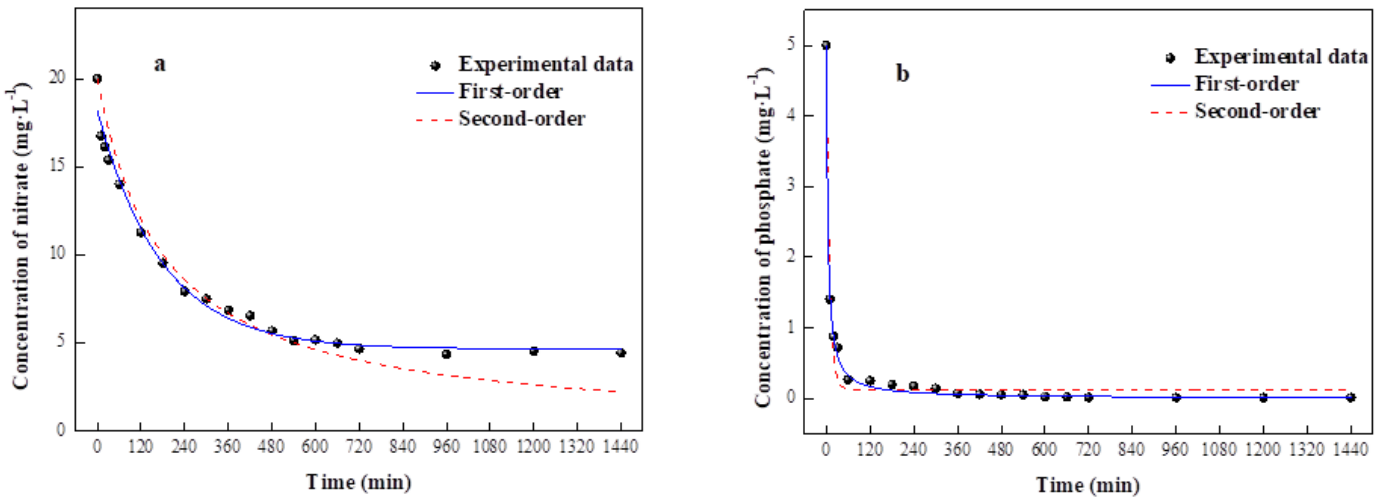

Figure 8

Kinetics of nitrate (a) and phosphate (b) removal (20 NO3−-N mg·L-1, 5 PO43-P mg·L-1, dosage = 2g·L-1, pH = 7, DO = 3 mg·L-1).

Supplementary Files

This is a list of supplementary files associated with this preprint. Click to download.

- Graphicalabstract.png
- Supplementarymaterial.docx